DOI 10.24425/aee.2024.149929

Effectiveness analysis of anti-galloping of spacer for catenary additional wires in strong wind section of high-speed railways

YOUPENG ZHANG[1], YAHUI ZHANG[1], SHANPENG ZHAO[1]✉, QIANG FENG[2], XIAOTONG YAO[1], NI YANG[1]

[1]*School of Automatic and Electrical Engineering, Lanzhou Jiaotong University China*

[2]*State Grid Ningxia Electric Power Company China*

e-mail: {zhang_youpeng/15838529560}@163.com, ✉ *zsp@mail.lzjtu.cn*

(Received: 11.01.2024, revised: 07.05.2024)

Abstract: To effectively suppress the violent galloping of the catenary additional wires in the strong wind section of high-speed railways, the anti-galloping effectiveness and anti-galloping mechanism of the spacer installed on the catenary additional wires are studied. Firstly, the finite element model of the additional wires of the catenary before and after the installation of the spacer is established. Secondly, the random wind field at the additional wires is simulated by the harmonic synthesis method (WAWS). Finally, the galloping response of the additional wires before and after the installation of the spacer is studied by using the finite element software. The results show that the installation of a single spacer at the midpoint of the span can reduce the vertical amplitude of the AF (Additional Feeder) and the PW (Protection Wire) by more than 39.80% and 41.51%, respectively, and the lateral amplitude decreases by more than 16.55% and 38.30%, respectively. The tension of the AF is greatly reduced, while the tension of the PW is slightly increased, so that the galloping of the AF and the PW tends to be synchronized. With the increase in the number of spacers installed, the anti-galloping effect continues to increase. At the same time, the anti-galloping mechanism of the spacer rod to suppress the vibration of the additional wires through the traction effect is clarified, and the effectiveness of the spacer rod in the anti-galloping of the additional wires of the catenary is proved.

Key words: anti-galloping measures, catenary additional wires, galloping response, high-speed railway, spacer

1. Introduction

With the large-scale construction of high-speed railways, a need to pass through the high wind section is inevitable. In many wind sections, the wind is frequent, strong and seasonal, resulting in frequent accidents such as train overturning, derailment and line sand burial [1,2]. For this reason, the wind wall protection project was built along the railway. Although the construction of the wind-break wall can effectively ensure the safe driving of the train, the wind-break wall "protects the train but does not protect the catenary". The blocking effect of the wall on the airflow causes a large galloping of the additional wires, which makes the distance between the AF (Additional Feeder) and the PW (Protection Wire) insufficient, thus causing discharge between the wires [3]. In addition, the severe galloping of the additional wires will also cause the wear of the wires strand, which is prone to accidents such as disconnection and catenary tripping, which has a serious impact on the safe operation of the electrified high-speed railway [4].

Scholars at home and abroad have conducted extensive research on the galloping problem of transmission lines by means of experiments, field investigation and simulation analysis. The research on the mechanism of wire galloping provides an important basis for solving the problem of transmission line galloping. Vertical excitation mechanism [5], torsional excitation mechanism [6,7] and eccentric inertia excitation mechanism [8,9], these mechanisms analyze the galloping factors of iced wires from different angles, which is of great significance for selecting appropriate anti-galloping measures and improving the stability of transmission lines. To prevent the galloping of transmission lines, Zhu Kuanjun and other scholars established a nonlinear static and dynamic calculation model of wire windage yaw, numerically simulated the asynchronous swing of transverse two-phase bundle wires, and studied the influence of installing interphase spacers on the displacement response and tension of wires. The results show that the installation of an interphase spacer can not only synchronize the swing between phase wires, but also effectively suppress the wind deflection amplitude of the wire [10]. Wang Liming and other scholars carried out experimental research on the UHV transmission line in the Jianshan test base in Henan Province, and proposed a new anti-galloping measure based on spacers, namely phase-to-ground spacers. The results show that the combined use of interphase and phase-to-ground spacers has a better effect on suppressing wire galloping [11]. Lou Wenjuan and other scholars analyzed the anti-galloping effect by studying the structural parameters and installation position of the turbulence anti-galloping device and the pneumatic damping plate [12]. In addition, in the prevention and control of wire galloping of overhead transmission lines, anti-galloping devices such as a detuning pendulum, shock hammer, spoiler and anti-galloping device are also applied. Many scholars have carried out in-depth research on the anti-galloping measures of transmission line. The structure of an electrified railway catenary is different from that of the power transmission line, and it has higher requirements for safety and reliability. Therefore, whether the existing anti-galloping scheme can be safely and effectively applied to the catenary additional wires still needs to be further studied.

In the study of wire galloping in the railway catenary, Zhang Hao and other scholars summarized a series of domestic and foreign literature related to catenary galloping, analyzed the research progress of catenary anti-galloping measures, summarized the problems to be solved in the study of catenary galloping, and put forward the contents and methods for further research [13]. Han Jiadong analyzed the galloping mechanism of catenary additional wires under strong wind

environment and proposed a series of galloping improvement measures, such as changing the constraint mode of additional wires and installing an anti-galloping device, but did not further analyze the effectiveness of the anti-galloping device [14]. Zhang Youpeng et al. analyzed the anti-galloping effect of the cable-stayed insulator on the AF of high-speed railways, and verified that the anti-galloping device had a good suppression effect on the galloping of the AF. However, the cable-stayed insulator is connected to the top of the wind-break wall and relies on the wind-break wall structure, which is unsuitable for catenary anti-galloping in other windy sections except high-speed railways [15]. The above scholars have proposed some anti-galloping measures for the catenary and its additional wires, but their safety and effectiveness research is still insufficient, and the widely recognized spacer anti-galloping device in the transmission line is widely recognized. There is little in-depth study on the application of catenary additional wires. Compared with the anti-galloping of iced wires on transmission lines, the additional wires of the catenary in windy sections are affected by unique airflow and operating environment, and the effective anti-galloping measures are very limited. It is necessary to carry out in-depth research on the anti-galloping effectiveness and anti-galloping mechanism of installing spacers on additional wires.

In this paper, aiming at the phenomenon of wind-induced galloping of catenary additional wires in the windy section of high-speed railways, based on the theory of fluid mechanics, the aerodynamic characteristics of catenary additional wires are analyzed. By establishing the finite element model of additional wires and a spacer anti-galloping device, the random wind field at the position of wires is simulated. The galloping response of additional wires before and after the installation of the spacer is studied from the aspects of wire amplitude, displacement spectrum and tension, and the suppression effect of the number and position of the spacer on the galloping is summarized. The anti-galloping mechanism of the spacer for the additional wires is clarified. The research results can provide important theoretical guidance for the anti-galloping of the spacer of the additional wires in the catenary of high-speed railways.

2. Catenary additional wires and spacer finite element modeling

2.1. Anti- galloping device of spacer

Most of the traction power supply systems of high-speed railways adopt AT power supply mode, and additional wires (AF and PW in this paper) need to be set up on the field side of the pillars [3]. The AF voltage is 27.5 kV, which has the functions of reducing a voltage drop, improving a power supply capacity and anti-electromagnetic interference. As for PW grounding, its main function is to protect the trip. Under the combined excitation of strong wind and windshield wall wake, the additional wire of a high-speed railway catenary gallops violently, as shown in Fig. 1.

The AF and PW potentials are different and are arranged in parallel in space, so spacers can be installed between the two wires to suppress galloping, as shown in Fig. 2. The spacer is essentially a composite insulator with mechanical strength and insulation performance. Because of its good anti-galloping effect, it is widely used in transmission lines [16]. In this paper, combined with the characteristics of additional wire space position, potential and environment, it is proposed to install a spacer anti-galloping device in the additional wire of the catenary to suppress the galloping of additional wires and ensure the safe operation of the traction power supply system.

(a) The highest point of galloping (b) The lowest point of galloping

Fig. 1. Galloping of additional wire of high-speed railway catenary in strong wind section

The spacer is mainly composed of a core rod and an insulating shed. The core rod is made of epoxy glass fiber, which has good insulation and mechanical properties. The main function of the umbrella sleeve is to protect the core rod and wire insulation, which has the function of preventing pollution flashover and wet flashover. The two ends of the spacer are hinged on the AF and PW, respectively, by connecting fittings, as shown in Fig. 3.

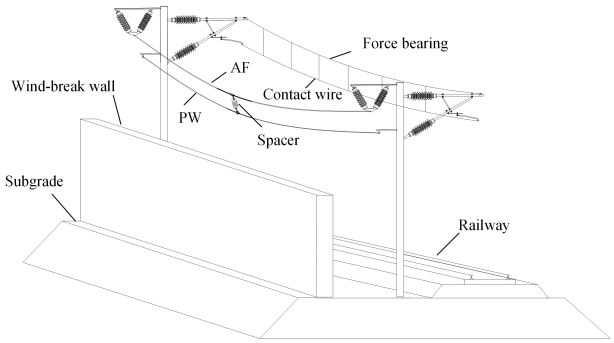

Fig. 2. Schematic diagram of installation of spacer for catenary additional wires

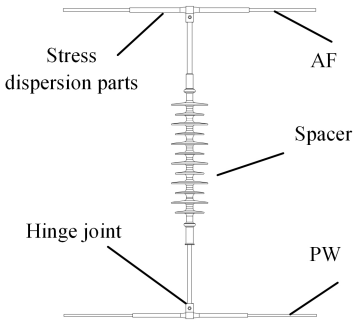

Fig. 3. Schematic diagram of spacer

2.2. Finite element modeling

Since the additional wire span of the high-speed railway catenary is generally 50 m, and there is almost no height difference between the two ends of the wire. The finite element model of additional wires is established by using finite element software. The wire only bears tension and its own gravity, and does not bear pressure and bending moment, so the LINK10 element is used to simulate the wire. The mechanical properties of the spacer are mainly determined by its core rod, and the influence of the shed can be ignored. Therefore, the BEAM188 unit is used to simulate the spacer. The unit properties are set according to the parameters shown in Table 1, and the self-weight analysis is carried out. The initial shape of the additional wire under a self-weight load is shown in Fig. 4(a). The initial shape of the additional wire after installing the spacer is shown in Fig. 4(b).

Table 1. The structural parameters of additional wires and spacer at 25°C

Wire parameters	**AF**	**PW**	**Spacer**	**Unit**
Wire type	LBGLJ-300/25	LBGLJ-120/35	FXGB-35	–
Rated tension	15	10	70	kN
Initial tension	3 662	2 502	0	N
Sectional area	333.31	156.49	706.5	mm^2
Elastic modulus	66.0	77.4	4	Gpa
Density	3 076.12	3 577.03	1 900	Kg/m^3

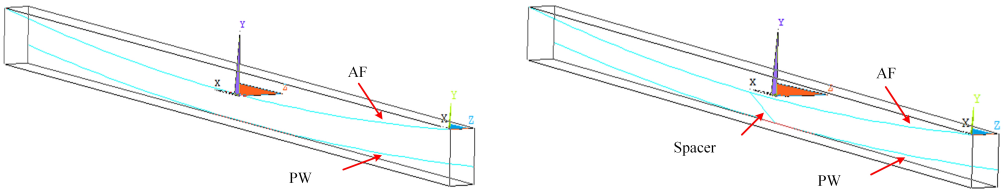

(a) No spacers installed (b) After installing the spacer

Fig. 4. Finite element model of additional wires before and after installation of spacer

The parabolic theory is used to calculate the initial configuration of the wire under a self-weight load [17].

$$z = \frac{qx(L-x)}{2H} + \frac{c}{L}x. \tag{1}$$

In the formula, q is the uniform self-weight load acting on the wire; L is the clue span; c is the height difference between the two ends of the suspension cable; H is the initial horizontal tension of the wire, which can be expressed as:

$$H = \frac{qL^2}{8f}. \tag{2}$$

In the formula, f is the mid-span sag of the wire.

In order to verify the rationality of the modeling, Table 2 shows the comparison between the simulation and theoretical results of the additional wire sag. The absolute error between the sag simulation value and the theoretical value is only 0.0003 m, which is less than 0.031 of the mid-span sag. It shows that the model in this paper is consistent with the actual structure.

Table 2. Comparison of simulation and theoretical results

Wire	AF	PW	Unit
Theoretical sag	0.9500	0.7490	m
Simulation sag	0.9503	0.7501	m

3. Aerodynamic load calculation and aerodynamic characteristics analysis of wires

3.1. Aerodynamic load calculation

At the height of the additional wires of the catenary, the wind velocity at any time t can be decomposed into average wind velocity and fluctuating wind velocity. The following equation:

$$U(ht) = \overline{U}(h) + v(ht). \tag{3}$$

When the fluid flows through the surface of the wires, an uneven pressure distribution will be generated, resulting in the combined effect of the flow resistance and the lift perpendicular to the flow direction on the unit wire [18]. To illustrate the force of the wires, the lift and resistance of the wires during the galloping process are shown in Fig. 5. θ is the angle between the relative wind velocity U_r and the incoming wind velocity U_x of the wires, $\dot{w}$ and $\dot{v}$ are the derivatives of the vertical and lateral displacements of the wires to time, that is, the lateral and vertical motion speeds of the wires, and $\dot{\beta}$ is the derivative of the torsion angle of the wires to time, that is, the torsion angular velocity of the wires.

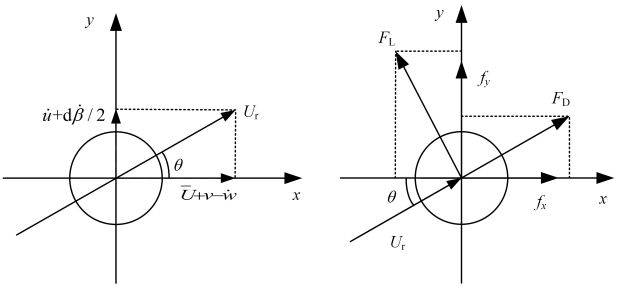

Fig. 5. Aerodynamic force diagram of additional wires

The lift and drag of the wires are expressed as [19]:

$$\begin{cases} F_L = (\rho D C_L U_r^2)/2 \\ F_D = (\rho D C_D U_r^2)/2 \end{cases}. \tag{4}$$

In the formula, F_L and F_D represent the lift and drag of the wires respectively, ρ represents the air density under standard pressure, D is the diameter of the additional wires, C_L and C_D represent the lift coefficient and drag coefficient, respectively, U_r represents the wind speed at the position of the wires.

The relative wind velocity U_r is expressed as:

$$U_r = \sqrt{(\overline{U} + v - \dot{w})^2 + (\dot{u} + d\dot{\beta}/2)^2}. \tag{5}$$

The relative wind attack angle θ is expressed as:

$$\theta = \tan^{-1} \frac{\dot{u} + d\dot{\beta}/2}{\overline{U} + v - \dot{w}}. \tag{6}$$

Among them, because the wires are not iced, the torsional angular velocity $\dot{\beta} = 0$.

In the actual situation, to better understand the force of the wires, according to the direction of the aerodynamic force on the additional wires of the catenary behind the wind-break wall, it can be converted into vertical and horizontal wind loads as follows:

$$\begin{cases} f_y = F_L \cos\theta + F_D \sin\theta \\ f_z = F_D \cos\theta - F_L \sin\theta \end{cases}. \tag{7}$$

Substituting Eqs. (4), (5) and (6) into Eq. (7), since the additional wires of the catenary is located in the wake growth section of the wind-break wall, the fluctuating wind velocity and the wires movement speed are smaller than the average wind velocity at the additional wires. Therefore, when calculating the component of the wind load per unit length of the additional wires, the product term and the higher order term of the fluctuating wind velocity and the wires motion speed can be ignored, and only the average wind velocity term can be considered. Thus, the components of the wind load per unit length of the additional wires on the y-axis and z-axis can be expressed as:

$$f_y = \rho C_L d\overline{U}(h)(\overline{U}(h) + 2v(ht))/2 - \rho d\overline{U}(h)(2C_L\dot{w} - C_D\dot{u})/2, \tag{8}$$

$$f_z = \rho C_D d\overline{U}(h)(\overline{U}(h) + 2v(ht))/2 - \rho d\overline{U}(h)(2C_D\dot{w} + C_L\dot{u})/2. \tag{9}$$

The first term on the right side represents the sum of wind loads, and the second term represents the aerodynamic damping of the wires. This paper focuses on the anti-galloping effect of the spacer. To simplify the calculation, the average wind velocity is set at the entrance of the calculation model, and the aerodynamic coefficient of the additional wires is measured, and the aerodynamic coefficient is calculated by taking the average value.

According to the aerodynamic load calculated by Formulas (8) and (9), the basic motion equation of the wire can be solved to obtain the galloping response of the additional wire. The basic dynamic equation of the additional wire of the catenary is:

$$\boldsymbol{M}\mathrm{d}^2\boldsymbol{u}/\mathrm{d}t^2 + \boldsymbol{C}\mathrm{d}\boldsymbol{u}/\mathrm{d}t + \boldsymbol{K}\boldsymbol{u} = \boldsymbol{F}(t). \tag{10}$$

In the formula, $\boldsymbol{M}$, $\boldsymbol{C}$ and $\boldsymbol{K}$ are the mass matrix, damping matrix and stiffness matrix of the structural unit, respectively. $\boldsymbol{u}$ is the displacement vector of the unit wire; $\boldsymbol{F}(t)$ is the element load vector.

3.2. Aerodynamic characteristics analysis

The fluid simulation software is used to simulate the wind speed and aerodynamic data of the additional wire position behind the wind wall under different wind speeds, and the Transition SST turbulence model is selected. In the simulation, the time step is 0.008 s, and the calculation is 1 000 steps. The SIMPLEC algorithm is used for the coupling of velocity and pressure. The pressure equation is discretized by second-order accuracy, and the momentum is discretized by a second-order upwind scheme. Along the high-speed railway, after the airflow is blocked by the embankment and the wind-break wall, the wind velocity in the wake section of the wind-break wall increases sharply to form a "wind surge" phenomenon, as shown in Fig. 6, and the AF and the PW are located in the growth zone, which is the direct cause of the large galloping of the additional wires. Considering the positive and negative alternating changes of the lift coefficient, the mean value is close to 0, so the root mean square value is used to characterize the lift coefficient, and the mean value is used to characterize the drag coefficient. The aerodynamic coefficient of the additional wire changes with the wind speed as shown in Fig. 7.

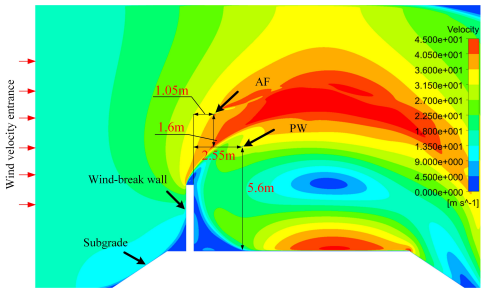

Fig. 6. Velocity cloud diagram of computational domain

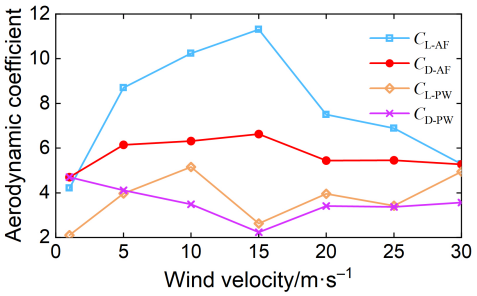

Fig. 7. The aerodynamic coefficient of additional wires varies with wind velocity

It can be seen from Fig. 7 that the overall change trend of the lift coefficient $C_{L-\mathrm{AF}}$ and the drag coefficient $C_{D-\mathrm{AF}}$ of the AF is consistent, both of which increase first and then decrease, and the lift coefficients and drag coefficients of the AF reach the peak when the wind velocity is 15 m/s. However, the variation of the lift coefficient $C_{L-\mathrm{PW}}$ and drag coefficient $C_{L-\mathrm{PW}}$ of the PW does not show a certain law, and its amplitude variation range is relatively small.

4. Wind tunnel test and simulation of random wind field

4.1. Wind tunnel test

According to the field observation data, the annual wind velocity in the windy section of high-speed railways is about 13.9~20.8 m/s. Therefore, the maximum wind velocity at the entrance is set to 27 m/s for the wind tunnel test. In this paper, the overall geometric similarity is considered when establishing the scale model of the wind tunnel test, and the similarity of load and dynamic characteristics is neglected [20]. The geometric similarity ratio of the test model is determined to be about 1:59, and the wind tunnel test model and wind velocity measurement device are shown in

Fig. 8 and Fig. 9. Under the wind tunnel test scale model, the wind velocity measuring instrument is used to monitor the velocity at the AF position under different inlet wind velocity, and the fluid simulation values are compared. The wind tunnel test results and numerical simulation values are shown in Table 3. According to the data in the table, the relative error between the measured value of the wind tunnel test and the simulated value is less than 5%, and the wind velocity at the AF position is about two times that of the incoming wind, which is consistent with the numerical simulation results. Therefore, the rationality and correctness of the model established in this paper are verified.

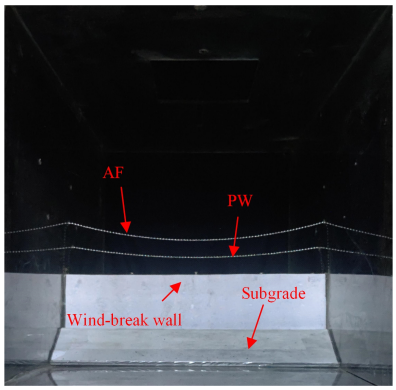

Fig. 8. Wind tunnel test model

Fig. 9. Anemometer

Table 3. Comparison of test results and simulation calculation under different inlet wind velocity

Inlet velocity/(m·s^{-1})	**The wind velocity at the AF position/(m·s^{-1})**	
	Test value	**Simulative value**
5.26	9.89	9.91
10.14	18.29	18.70
16.75	31.71	30.50
20.40	38.50	37.00
22.13	42.80	40.08
26.41	51.94	49.45

4.2. Wind field simulation

According to the field observation and literature data, it can be seen that the overhead wires show asynchronous galloping, which easy reduces the distance between the phases of each phase wires, resulting in discharge, tripping and other accidents. Applying random wind loads to overhead wires can accurately simulate the non-synchronous galloping of transmission lines [11].

The harmonic synthesis method is a method of simulating and modeling the random process by using spectral decomposition and trigonometric function superposition. The power spectral density of the wind velocity time history obtained by this method is basically consistent with the target value, and the fluctuation variance is also close to the theoretical value [21]. Therefore, this paper uses the harmonic synthesis method to simulate and analyze the wind field of the catenary additional wires. The fluctuating wind power spectrum adopted by the current structural wind resistance design code in China is the Davenport power spectrum [22], and its expression is:

$$S_v(n) = \overline{v}_{10}^2 \frac{4kx^2}{n(1+x^2)^{4/3}}, \tag{11}$$

$$x = 1200n/\overline{v}_{10}. \tag{12}$$

In the equation, $S_v(n)$ is the wind velocity power spectrum; n is the frequency; k is the roughness coefficient; $\overline{v}_{10}$ is the average wind velocity at a height of 10 m from the ground.

The inlet wind velocity is set to 15 m/s, and the wind velocity time history curve at the additional wires' position obtained by simulation is shown in Fig. 10. It can be seen from the Figure that the wind velocity at the position of the AF and the PW is 2.2 times and 1.2 times of the wind velocity under the initial conditions, which is consistent with the results of the fluid numerical simulation calculation and the wind tunnel test, indicating that the fluctuating wind function can better simulate the real wind velocity at the position of additional wires under the wake of the wind-break wall.

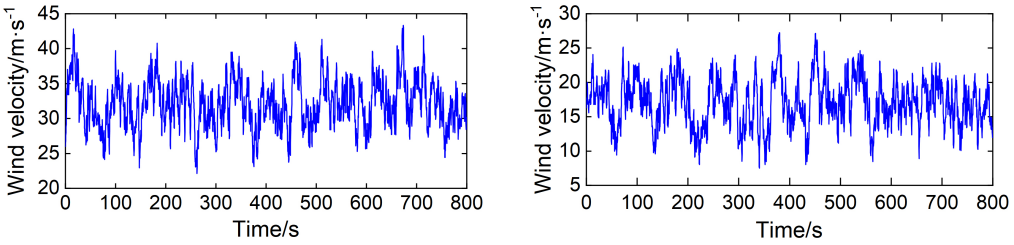

(a) AF (b) PW

Fig. 10. Wind velocity histories curve at the position of the additional wires

5. Analysis of anti-galloping effect of spacer

This paper first installs the spacer at the midpoint of the additional wires span, and discusses the anti-galloping effect of the spacer under a wind velocity of 10~25 m/s, which is the most violent galloping of the additional wires in the field. The transient dynamics module in the fluid mechanics software is used for simulation analysis. The calculated aerodynamic load is applied to each element node of the wires. The Newmark method is used to solve the nonlinear dynamic equilibrium equation of the AF and the PW under each wind velocity. The time step is set to 0.008 s. The number of iterations is 25, and the calculation time is 800 s. This paper selects 15 m/s wind velocity as an example for analysis, and other galloping data are listed in tabular form.

5.1. Amplitude analysis

Figure 11 shows the displacement time history of the midpoint of the additional wires span before and after the installation of the spacer when the inlet wind velocity is 15 m/s. The initial displacement values of AF and PW are defaulted to 0m. The vertical amplitude of the AF before the installation of the spacer is 1.74 m, and the lateral amplitude is 1.80 m. The vertical amplitude of the PW is 1.59 m, and the lateral amplitude is 1.92 m. At this time, the additional wires gallop violently. After the installation of the spacer, due to the constraint of the midpoint freedom of the additional wires, the time-history curves of the midpoint displacement of the two wires are the same. The vertical amplitude of the AF and the PW decrease to 0.93 m, and the lateral amplitude decrease to 1.03 m indicate that the spacer can effectively suppress the galloping of the additional wires.

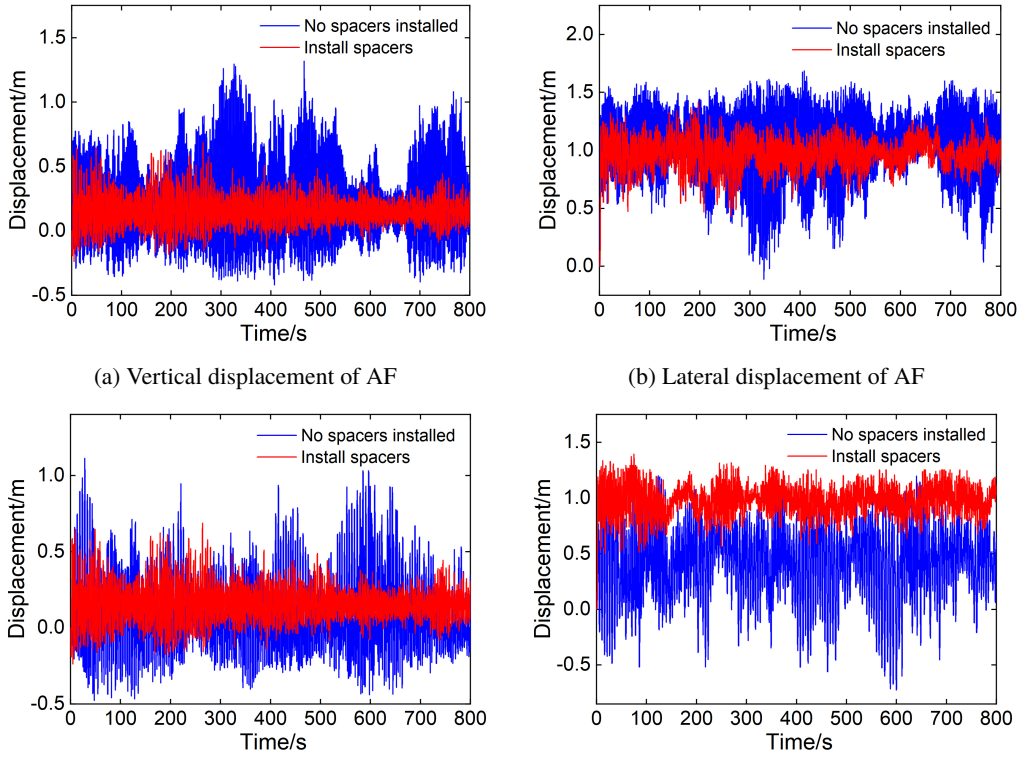

(a) Vertical displacement of AF

(b) Lateral displacement of AF

(c) Vertical displacement of PW

(d) Lateral displacement of PW

Fig. 11. Displacement of additional wires before and after installation of spacer

To test the effect of galloping prevention after the installation of spacers, the damping rate equation shown in Eq. (13) is used to evaluate:

$$\lambda = \frac{A_b - A_a}{A_b} \times 100\%. \tag{13}$$

In the equation, A_b is the amplitude of the wires before installing the spacer, and A_a is the amplitude of the wires after installing the spacer.

The amplitude and vibration reduction rate of the wires before and after the installation of the spacer at the midpoint of the additional wires span are simulated and analyzed respectively. The calculation results are shown in Table 4.

Table 4. Comparison of additional wires amplitude before and after installation of spacer

Wires	**Wind velocity/m·s^{-1}**	**Vertical amplitude/m**		**Lateral amplitude/m**		**Damping rate λ /%**	
		Before	**After**	**Before**	**After**	**Vertical**	**Lateral**
AF	10	1.32	0.67	1.39	1.16	49.24	16.55
	15	1.74	0.93	1.80	1.03	46.55	42.78
	20	1.59	0.73	1.81	1.12	54.09	38.12
	25	0.98	0.59	1.94	1.56	39.80	19.59
PW	10	1.41	0.67	1.88	1.16	52.48	38.30
	15	1.59	0.93	1.91	1.03	41.51	46.07
	20	2.35	0.73	2.56	1.12	68.93	56.25
	25	2.67	0.59	2.81	1.56	78.07	44.48

It can be seen from the data in the table that when the wind velocity is 20 m/s and 25 m/s, the installation of the spacer anti-galloping device has a significant effect on suppressing the galloping of the additional wires. At a wind velocity of 20 m/s, the spacer anti-galloping device can reduce the vertical amplitude and lateral amplitude of the AF by 54.09% and 38.12%, respectively, and the vertical amplitude and lateral amplitude of the PW are reduced by 68.93% and 56.25%, respectively. Under a wind velocity of 25 m/s, the vertical amplitude and lateral amplitude of the AF are reduced by 39.80% and 19.59%, respectively, and the vertical amplitude and lateral amplitude of the PW are reduced by 78.07% and 44.48%, respectively. It shows that in the case of large wind velocity, the spacer anti-galloping device still has a significant anti-galloping effect. Therefore, the spacer anti-galloping device can effectively suppress the galloping of the additional wires of the catenary under different wind velocity.

5.2. Spectrum analysis

The existing research results show that under certain conditions, there is a certain correlation between the frequency of galloping and the natural frequency of the wire, that is:

$$f = f_n = \frac{n}{2l}\sqrt{\frac{T}{m}}. \tag{14}$$

where n denotes the order of vibration; l denotes the span of the wire; m represents the mass per unit length of the wires; T represents the wires' tension.

Through Eq. (14), the first-order natural frequency of the AF is 0.549 Hz, and the first-order natural frequency of the PW is 0.585 Hz. At the same time, the displacement data of the additional

wires before the installation of the spacer rod are processed by Fast Fourier Transform (FFT). The vertical displacement spectrum change of the additional wires can be obtained. As shown in Fig. 12 and Fig. 13, the displacement spectrum of the AF and the PW is 0.552 Hz and 0.594 Hz, respectively, in the first-order natural frequency, which is close to the calculated value of Eq. (14). Its second-order natural frequency has peaks near 1.098 Hz and 1.171 Hz, indicating that the galloping mode is dominated by first-order galloping and there is a certain second-order galloping. It can be seen that the numerical simulation value is close to the calculated natural frequency of the additional wires.

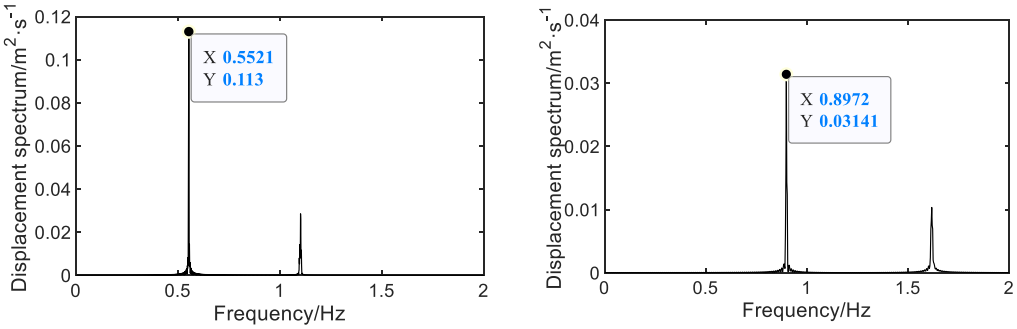

(a) Before installing the spacer (b) After installing the spacer

Fig. 12. Displacement spectrum of AF before installation of spacer

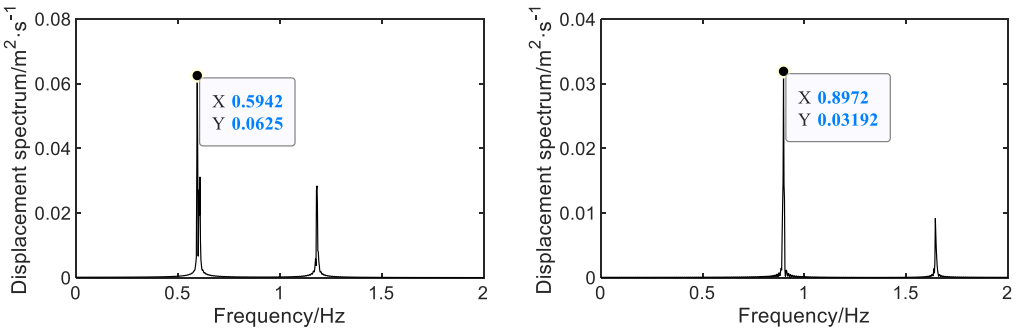

(a) Before installing the spacer (b) After installing the spacer

Fig. 13. Displacement spectrum of PWs before installation of spacer

Comparing the galloping displacement spectrum changes of the AF and the PWs after the installation of the spacer, it can be seen that the main frequency of the additional wires after the installation of the spacer anti-galloping device increases to 0.897 Hz, and the spectrum amplitude also shows a significant decrease, which also proves that the spacer has a significant anti-galloping effect.

5.3. Tension analysis

Before and after the installation of the spacer anti-galloping device, the tension of the additional wires will also show a certain change. Figure 14 shows the tension change curve of the additional wires before and after the installation of the spacer anti-galloping device. Table 5 shows the change data of tension of additional wires before and after the installation of the spacer.

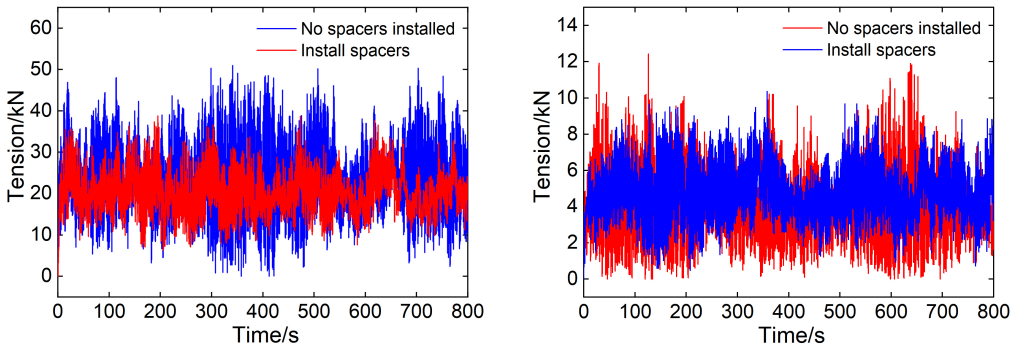

(a) AF (b) PW

Fig. 14. Time histories of tension before and after installation of spacer for additional wires

Table 5. Comparison of tension of additional wires before and after installation of spacer

Wires	spacer	Average value/N	Standard deviation	Maximum value/N
AF	Before	22 886.18	8 581.71	50 951.47
	After	20 454.14	5 156.96	38 811.14
PW	Before	3 589.14	1 432.24	10 367.08
	After	6 685.43	2 073.45	12 505.21

By comparing the statistical data of the additional wires' tension before and after the installation of the spacer, it can be seen that before the installation of the spacer, the additional wires' tension fluctuated significantly, and the maximum tension of the AF reaches 50 951.47 N, while the maximum tension of the PW is 10 367.08 N. After installing the spacer anti-galloping device, the maximum tension of the AF decreases by 12 140.33 N, and the maximum tension of the PW increases by 2 138.13 N; the standard deviation of the AF is reduced by 3 424.75, and the standard deviation of the PW is increased by 641.20. At the same time, the average tension decreased to 20 454.14 N, and the average PW increased to 6 685.43 N. The increase in the tension of the PW is due to the obvious increase in the lateral displacement of the PW after the installation of the spacer (as can be seen in Fig. 11(d)). It can be seen that the installation of the spacer can greatly reduce the tension of the AF, and the tension of the PW increases slightly, which reflects the anti-galloping mechanism that the spacer transfers the vibration of the AF to the PW through the pulling effect. It shows that the spacer anti-galloping device has obvious balance and improvement effect on the additional wires' tension.

6. Analysis of the number and position of spacer installation

Through the above spectrum analysis, it can be seen that the additional wire galloping mode is mainly the first-order galloping, and there is a certain second-order galloping. To further study the scheme of enhancing the anti-galloping effect of spacers, it is considered to further suppress the second-order galloping while suppressing the first-order galloping of additional wires. For this reason, a wind velocity of 15 m/s is selected, and two spacers are installed at 1/3 and 2/3 positions of the AF and the PW, and three spacers are installed at 1/4, 1/2 and 3/4 positions. The number and position of spacers are shown in Fig. 15. The influence of the number and installation position of spacers on the anti-galloping effect is compared and analyzed.

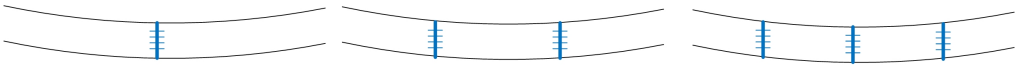

(a) 1 spacer (b) 2 spacers (c) 3 spacers

Fig. 15. Installation number and position of spacers

6.1. Amplitude analysis

Figure 16 is the analysis diagram of the influence of the number of spacers installed on the galloping amplitude of the additional wires of the catenary. With the increase in the number of spacers installed, the vertical amplitude reduction rate and lateral amplitude reduction rate of the AF can reach 50.57% and 53.89% respectively, and the vertical amplitude reduction rate and lateral amplitude reduction rate of the PW can reach 45.91% and 56.54% respectively. When two spacers are installed, the vibration reduction rate of the AF and the PW is reduced due to the fact that the spacers are installed at 1/3 and 2/3 positions of the AF and the PW, and the degree of freedom at the midpoint of the wire is slightly increased. On the whole, with the increase in the number of installed spacers, the vibration reduction rate of the additional wires shows an upward trend, indicating that increasing the number of installed spacers can continuously reduce the galloping amplitude of the additional wires of the catenary.

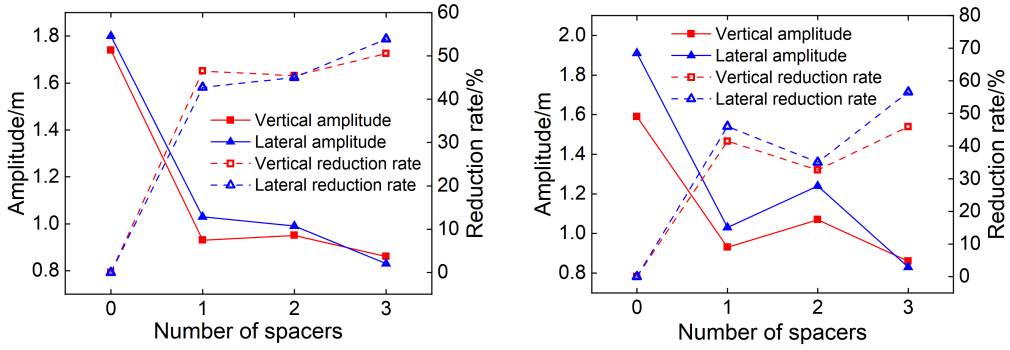

(a) AF (b) PW

Fig. 16. Effect of the number of spacers installed for the galloping amplitude of additional wires

6.2. Tension analysis

Figure 17 is the analysis diagram of the influence of the number of phase spacers installed on the additional wires' tension of the catenary. From the diagram, it can be seen that with the increase in the number of spacers installed, the maximum tension of the AF continues to decrease by 15 146.82 N, the standard deviation continues to decrease by 3 761.64, and the average value continues to decrease to 18 240.43 N. The maximum tension of the PW continues to increase by 5 584.19 N, the standard deviation continues to increase by 802.41, and the mean value continues to increase to 8 078.54 N. This shows that with the increase in the number of spacers installed, the AF is continuously increased by the traction of the spacer and the PW, the tension continues to decrease, and the stability gradually increases; the influence of the AF on the PW continues to increase, and the tension and its fluctuation continue to increase slightly. It can be seen that the installation of the spacer has obvious pulling effect on the PW and the AF, indicating that the installation of the spacer can significantly enhance the overall stability of the catenary additional wires.

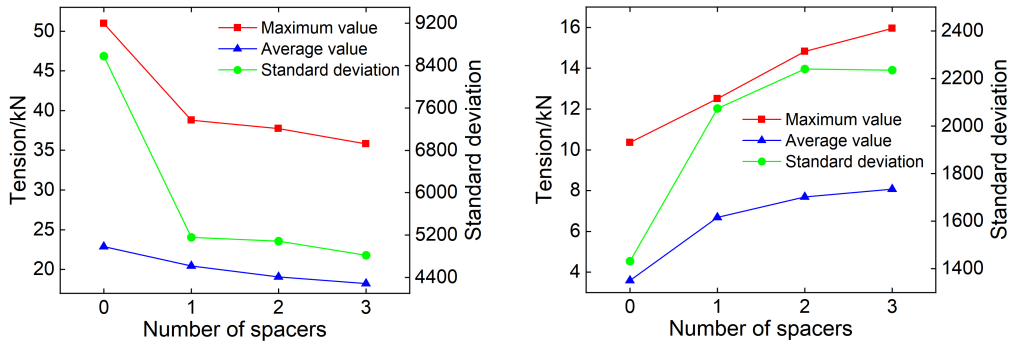

(a) AF (b) PW

Fig. 17. Effect of the number of spacers installed on the tension of additional wires

Figure 18 is the time history diagram of the tension of the spacer at the midpoint of the span when installing one spacer and three spacers on the additional wires. From the diagram, it can be seen that the tension of the spacer rod has both positive and negative values, indicating that the spacer rod is not only subjected to the tension generated when the AF and the PW are far away from each other, but also the pressure generated when the AF and the PW are close to each other. It is shown that the galloping state of the AF and the PW under random wind load excitation is asynchronous galloping, which is basically the same as the galloping process observed in the actual wire. Further analysis of the variation law of the spacer tension time history curve found that with the change of time, the absolute value of the tension of the spacer has a decreasing trend, and this trend is more significant when the number of installed spacers reaches three. It shows that the installation of spacers can synchronize the galloping of AF and PW so as to avoid too small distance and reduce the probability of accidents such as discharge and tripping. In addition, the absolute value of the maximum tension of the time spacers installed with one and three spacers is 1.926 kN and 0.965 kN, respectively, which is much smaller than the design-rated tension of spacers of 70 kN. It shows that the spacer is a safe and effective anti-galloping measure.

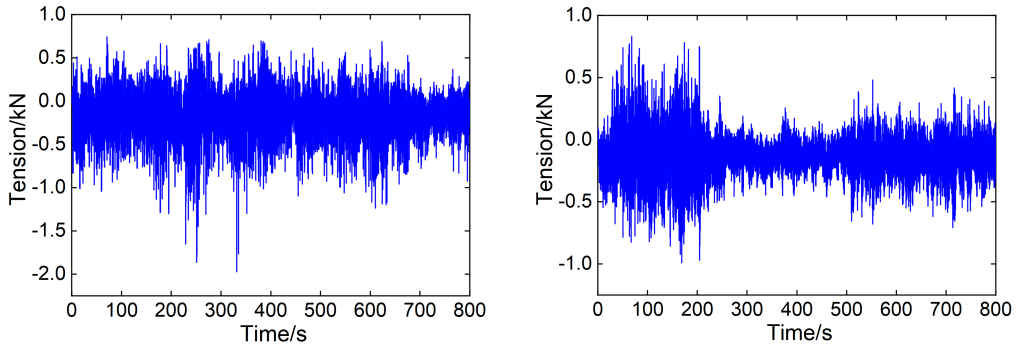

(a) 1 spacer (b) 3 spacers

Fig. 18. Time history change of span midpoint spacer tension

By comparing the data on the influence of the number of spacers on the amplitude and tension of the additional wires, it can be seen that after installing a spacer, the damping effect of the AF and the PW decrease obviously. After installing two or three spacers, the damping effect of the AF and the PW continues to increase, but the increase tends to be gentle. Considering the balance between economic benefit and anti-galloping effect, it is suggested that the number of spacers should be selected according to the wind section, wind force and galloping intensity of the wire in the strong wind section of high-speed railways, so as to improve the overall stability of the additional wires.

7. Conclusion

1. After installing a spacer at the midpoint of the span, the vertical amplitude reduction rates of the AF and the PW are more than 39.80% and 41.51%, respectively, up to 54.09% and 78.07%, respectively. The lateral amplitude decreases by more than 16.55% and 38.30%, respectively, up to 42.78% and 56.25%, respectively. The main frequency of the additional wires is greatly increased, and with the increase in wind velocity, the anti-galloping effect of the spacer is still significant.
2. After the spacer is installed, the tension of the AF is greatly reduced, and the tension of the PW is slightly increased, which reflects the anti-galloping mechanism that the spacer transfers the vibration of the AF to the PW through the pulling effect. It shows that the spacer anti-galloping device has obvious balance and improvement effect on the additional wires' tension.
3. The AF and the PW have asynchronous galloping under a random wind load. The installation of spacers can make the galloping of the AF and the PW tend to be synchronized, thereby avoiding too small distance, and reducing the probability of accidents such as discharge and tripping. With the increase in the number of spacers installed, this effect is more significant. In addition, the safety of the spacer anti-galloping device is proved by analyzing the tension of the spacer.

4. Increasing the number of installed spacers to two or three can further reduce the galloping amplitude of the additional wires of the catenary and improve the stability of the additional wires structure, but the vibration reduction effect tends to be gentle. Considering the balance between economic benefits and anti-galloping effect, it is suggested that the number of spacers should be selected according to the galloping intensity of the wire in the windy section of high-speed railways.

Acknowledgements

This research was financially supported by the National Natural Science Foundation of China (51867013) and the Science and Technology Research and Development Program of China Railway Beijing Group Co., Ltd. (2024AGD03).

References

[1] Huang S.L., *Research on the wind break standard of Lanzhou-Urumqi high-speed railway*, Journal of Railway Engineering, vol. 36, no. 6, pp. 14–17 (2019), DOI: 10.3969/j.issn.1001-4632.2016.03.19.

[2] Tian R., Zhang J.Q., Lu M., *Research on the influence of power frequency electric field of pantograph on passengers' health in high-speed EMU*, Archives of Electrical Engineering, vol. 72, no. 3, pp. 483–501 (2023), DOI: 10.24425/aee.2023.145421.

[3] Han J.D., *Research on galloping mechanism and protective measures of high-speed railway catenary additional wire in windy area*, Railway Standard Design, vol. 59, no. 12, pp. 125–129 (2015), DOI: 10.13238/j.issn.1004-2954.2015.12.029.

[4] Zhao S.X., *Research on galloping online monitoring and condition assessment for catenary positive feeder of Lanzhou-Urumqi high-speed railway in gale area*, MA. Eng. Thesis, Lanzhou Jiaotong University, Lanzhou, China (2021).

[5] Denhartog J.P., *Transmission line vibration due to sleet*, AIEE Transactions, vol. 51, no. 4, pp. 1074–1076 (1932), DOI: 10.1109/T-AIEE.1932.5056223.

[6] Nigol O., Buchan P.G., *Conductors galloping 1: Den Hartog mechanism*, IEEE Transactions on Power Apparatus and Systems, vol. 100, no. 2, pp. 699–707 (1981), DOI: 10.1109/TPAS.1981.316921.

[7] Nigol O., Buchan P.G., *Conductors galloping 2: torsional mechanism*, IEEE Transactions on Power Apparatus and Systems, vol. 100, no. 2, pp. 708–720 (1981), DOI: 10.1109/TPAS.1981.316922.

[8] Yu P., Popplewell N., Shah A.H., *Instability trends of inertially coupled galloping: part I: Initiation*, Journal of Sound and Vibration, vol. 183, no. 4, pp. 663–67 (1995), DOI: 10.1006/jsvi.1995.0278.

[9] Yu P., Popplewell N., Shah A.H., *Instability trends of inertially coupled galloping: part II: Periodic vibrations*, Journal of Sound and Vibration, vol. 183, no. 4, pp. 679–691 (1995), DOI: 10.1006/jsvi.1995.0179.

[10] Wang L.M., Gao Y.Y., Lu M., *Calculation on a new anti-galloping technique for UHV transmission lines*, High Voltage Technology, vol. 43, no. 8, pp. 2541–2550 (2017), DOI: 10.13336/j.1003-6520.hve.20170731014.

[11] Zhu K.J., Di Y.X, Li X.M., *Analysis of overhead transmission line for asynchronous swaying by the finite element method*, High Voltage Technology, vol. 36, no. 4, pp. 1038–1043 (2010), DOI: 10.13336/j.1003-6520.hve.2010.04.005.

[12] Lou W.J., Sun Z.M., Lu Y., *Anti-galloping effects of air flow spoiler and aerodynamic damping board*, Power Grid Technology, vol. 34, no. 2, pp. 200–204 (2010), DOI: 10.13335/j.1000-3673.pst.2010.02.032.

[13] Zhang H., Xie Q., *Researches on wind-induced galloping of electric railway catenary*, Railway Standard Design, vol. 59, no. 9, pp. 145–148 (2015), DOI: 10.13238/j.issn.1004-2954.2015.09.032.

[14] Han J.D., *Study on mechanism of high-speed railway catenary additional wire dancing in strong wind area and protective measures*, Railway Standard Design, vol. 59, no. 12, pp. 125–129 (2015), DOI: 10.13238/j.issn.1004-2954.2015.12.

[15] Zhang Y.P., Zhang C.R., Zhao S.P., *Anti-galloping effectiveness analysis of positive feeder cable-stayed insulator of catenary in strong wind area of Lanzhou-Urumqi high-speed railway*, High Voltage Technology, vol. 46, no. 11, pp. 3905–3913 (2020), DOI: 10.13336/j.1003-6520.hve.20200104.

[16] Cui W., Yan B., Yang X.H., *Numerical investigation on anti-galloping of double bundle conductors with interphase spacers*, Vibration and Shock, vol. 33, no. 20, pp. 47–51 (2014), DOI: 10.13465/j.cnki.jvs.2014.20.010.

[17] Yang F.L., Yang J.B., Zhang Z.F., *Analysis on the dynamic responses of a prototype line from iced broken conductor*s, Engineering Failure Analysis, vol. 39, no. 1, pp. 108–123 (2014), DOI: 10.1016/j.engfailanal.2014.01.01.

[18] Zhao S.P., Ge W., Wang S.H., *Effectiveness analysis of new triangle anti-galloping device for catenary additional conductors in strong wind section of Lanzhou-Xinjiang high-speed railway*, High Voltage Technology, vol. 48, no. 12, pp. 4852–4862 (2022), DOI: 10.13336/j.1003-6520.hve.20211436.

[19] Nguyen V.L., Ho D.K., *Numerical investigation of vortex wake patterns of laminar flow around two side-by-side cylinders*, Archive of Mechanical Engineering, vol. 69, no. 3, pp. 541–565 (2022), DOI: 10.24425/ame.2022.141517.

[20] Wang W.J., *Experimental study on amplitude death mechanism of the dynamic system of transmission line*, MA. Eng. Thesis, Hunan University of Science and Technology, Changsha, China (2019).

[21] Liu Z.G., Hou Y.C., Han Z.W., *Analysis on dynamic characteristics of high-speed railway catenary based on wind field simulation*, Journal of Railway, vol. 35, no. 11, pp. 21–28 (2013), DOI: 10.3969/j.issn.1001-8360.2013.11.004.

[22] Luo G.J., Zhu H.Z., Li P., *Simulation research on stochastic wind field of offshore wind turbine based on harmonic superposition method*, Journal of Wuhan University of Technology, vol. 43, no. 3, pp. 42–48 (2021).